Development 139, 1316-1326 (2012) doi:10.1242/dev.074344

A zebrafish model of lethal congenital contracture syndrome 1 reveals Gle1 function in spinal neural precursor survival and motor axon arborization

Li-En Jao[1], Bruce Appel[2] and Susan R. Wente[1,*]

SUMMARY

In humans, *GLE1* is mutated in lethal congenital contracture syndrome 1 (LCCS1) leading to prenatal death of all affected fetuses. Although the molecular roles of Gle1 in nuclear mRNA export and translation have been documented, no animal models for this disease have been reported. To elucidate the function of Gle1 in vertebrate development, we used the zebrafish (*Danio rerio*) model system. *gle1* mRNA is maternally deposited and widely expressed. Altering Gle1 using an insertional mutant or antisense morpholinos results in multiple defects, including immobility, small eyes, diminished pharyngeal arches, curved body axis, edema, underdeveloped intestine and cell death in the central nervous system. These phenotypes parallel those observed in LCCS1 human fetuses. Gle1 depletion also results in reduction of motoneurons and aberrant arborization of motor axons. Unexpectedly, the motoneuron deficiency results from apoptosis of neural precursors, not of differentiated motoneurons. Mosaic analyses further indicate that Gle1 activity is required extrinsically in the environment for normal motor axon arborization. Importantly, the zebrafish phenotypes caused by Gle1 deficiency are only rescued by expressing wild-type human GLE1 and not by the disease-linked Fin_{Major} mutant form of GLE1. Together, our studies provide the first functional characterization of Gle1 in vertebrate development and reveal its essential role in actively dividing cells. We propose that defective GLE1 function in human LCCS1 results in both neurogenic and non-neurogenic defects linked to the apoptosis of proliferative organ precursors.

KEY WORDS: mRNA metabolism, Neurodegeneration, Zebrafish

INTRODUCTION

Arthrogryposis multiplex congenita (AMC) is a heterogeneous group of human disorders with an estimated worldwide incidence of 1 in 3000 births (Hall, 1985). It is, however, more common in genetically isolated groups such as the Finnish and Israeli Bedouin populations (Lebenthal et al., 1970; Pakkasjarvi et al., 2006). To date, over 150 AMC conditions varying in etiology, pathogenesis and other organ anomalies have been described with multiple deformities of the joints (contractures) at birth being the predominant shared symptom (Hall, 1997). Among these AMC conditions, lethal congenital contracture syndrome 1 (LCCS1) is a distinct entity and one of the most severe forms manifested in utero, with prenatal death of all affected fetuses by week 32 of gestation (Herva et al., 1985; Makela-Bengs et al., 1998). LCCS1 is an autosomal recessive disorder that was originally reported in ten families from northeastern Finland (Herva et al., 1985). Affected LCCS1 fetuses show joint contractures, early loss of voluntary muscle movement, small jaws (micrognathia), incomplete lung development and muscular atrophy (Herva et al., 1985). Of note, LCCS1 fetuses exhibit a distinct neuropathology with marked loss of the ventral spinal cord, both in the anterior-horn motoneurons and the ventral and lateral funiculi (with less alteration of the sensory nuclei and the dorsal funiculus) (Herva et al., 1988). These observations have led to speculation that the LCCS1 pathology is due to defects in motoneuron development and maturation.

Recently, a genetic study linked *GLE1* mutations to LCCS1 (Nousiainen et al., 2008). The major mutation, Fin_{Major}, is a single-nucleotide substitution that generates an illegitimate splice acceptor site in intron 3, producing a three amino acid insertion in the human GLE1 protein. Gle1 was first identified as an essential mRNA export factor in both *S. cerevisiae* and human cells (Kendirgi et al., 2003; Murphy and Wente, 1996; Watkins et al., 1998). In addition to mRNA export, we recently discovered a novel role for Gle1 in mediating efficient translation initiation and termination (Bolger et al., 2008). This work, together with substantial biochemical and cell biological analysis of Gle1 function (reviewed by Folkmann et al., 2011), reveals that Gle1 is a key regulator of multiple post-transcriptional gene expression steps. To date, no studies of the role of Gle1 in vertebrate development have been reported. Moreover, a specific role for Gle1 in motoneuron development has not been documented.

Here we investigate the link between Gle1 function and LCCS1 pathology using zebrafish (*Danio rerio*) as a model system. Using a *gle1* insertional mutant line and an antisense morpholino knockdown strategy, we show that disrupting Gle1 function leads to morphological anomalies that parallel key phenotypes of LCCS1 human fetuses. Gle1 depletion also results in reduced spinal cord motoneurons, and Gle1 activity is required extrinsically in the environment for motor axon arborization. Surprisingly, motoneuron reduction is caused by apoptosis of neural precursors, rather than acute motoneuron death. This directly contrasts with the previously proposed LCCS1 pathophysiological mechanism (Nousiainen et al., 2008). Based on this first functional characterization of Gle1 in

[1]Department of Cell and Developmental Biology, Vanderbilt University School of Medicine, U-3209 MRBIII, 465 21st Avenue South, Nashville, TN 37232-8240, USA. [2]Department of Pediatrics, University of Colorado School of Medicine, Aurora, CO 80045, USA.

*Author for correspondence (susan.wente@vanderbilt.edu)

Accepted 25 January 2012

vertebrate development, we propose that rapidly dividing cells, including the organ precursors in both neuronal and non-neuronal tissues, have a high demand for Gle1 activity as they undergo proliferation. As a result of Gle1 deficiency, the death of proliferative organ precursors during early embryonic development is likely to be the common underlying cellular mechanism that leads to the pleiotropic abnormalities in affected LCCS1 fetuses.

MATERIALS AND METHODS

Zebrafish lines and genotyping

Wild-type AB and *gle1*^{hi4161a} zebrafish (*Danio rerio*) strains were bred and maintained using standard procedures (Westerfield, 2000). Embryos were obtained by natural spawning and staged according to Kimmel et al. (Kimmel et al., 1995). We used transgenic line *Tg(gfap:GFP)* (Bernardos and Raymond, 2006) and generated lines *Tg(mnx1:TagRFP-T)* and *Tg(mnx1:H2A-TagRFP-T)* (see below). In some cases, 0.003% (w/v) 1-phenyl-2-thiourea (PTU) was added to the medium to block trunk pigmentation. Wild-type, heterozygous and homozygous *gle1*^{hi4161a} embryos were genotyped using a three-primer PCR strategy (Wang et al., 2007) (see supplementary material Table S1 for primers).

Plasmids

To clone zebrafish *gle1*, total RNA was isolated from wild-type AB embryos (shield stage) using TRIzol (Invitrogen, Carlsbad, CA, USA). cDNA was made from 2 μg total RNA by reverse transcription using an oligo(dT)$_{16}$ primer (Roche Diagnostics, Indianapolis, IN, USA) and SuperScript III reverse transcriptase (Invitrogen). The coding sequences for zebrafish *gle1a* and *gle1b* were amplified from cDNA using Phusion high-fidelity DNA polymerase (New England Biolabs, Ipswich, MA, USA) with specific primers (supplementary material Table S1) for insertion into pDONR221 using Gateway BP Clonase II enzyme mix (Invitrogen) to generate *pME-drgle1a* and *pME-drgle1b*.

Zebrafish *mnx1* upstream elements were PCR amplified from purified wild-type zebrafish genomic DNA using Phusion high-fidelity DNA polymerase with specific primers (supplementary material Table S1) and inserted into pDONRP4-P1R using Gateway BP Clonase II enzyme mix to generate *p5E-mnx1*. *p5E-mnx1* contains the 5136 bp upstream elements of *mnx1*, including the non-coding sequence of the first exon.

The plasmid *pCMV/SP6-hsGLE1b* with human *GLE1b* driven by the CMV/SP6 promoter was generated by MultiSite Gateway cloning (Kwan et al., 2007) using the PCR-amplified human *GLE1b* sequence (Kendirgi et al., 2005). For the Fin$_{Major}$ mutation, we performed standard PCR-based site-directed mutagenesis (Braman et al., 1996) using plasmid *pCMV/SP6-hsGLE1b* to insert CCTTTTCAG between positions 432 and 433 of the coding DNA.

Histology

In situ hybridizations were performed as described (Thisse and Thisse, 2008). Digoxygenin-labeled *gle1* antisense RNA probes (Roche Diagnostics) were prepared from *Dra*I-linearized zebrafish *gle1* plasmid using SP6 RNA polymerase. Embryos were cleared in serial incubations of glycerol (25, 50 and 75%) before imaging.

Whole-mount immunohistochemistry was performed as described (Sarmah et al., 2005). Indirect immunofluorescence was performed using the following antisera: anti-Islet1/2 [39.4D5, Developmental Studies Hybridoma Bank (DSHB), University of Iowa; 1:200]; anti-zn-8 (DSHB; 1:200); anti-Elavl (16A11, Invitrogen; 1:250); anti-cleaved caspase 3 (Abcam, Cambridge, MA, USA; 1:500); and anti-Sox2 (Abcam; 1:500). Alexa Fluor-conjugated secondary antibodies (Invitrogen) were used.

For cryosections, fixed embryos were embedded in 1.5% agarose/5% sucrose, equilibrated in 30% sucrose and frozen in a 2-methyl-butane/liquid nitrogen bath. Blocks were sectioned (10 μm) using a Leica CM3050 cryostat. Antibody staining of cryosections was performed as for the whole-mount procedure with no detergent added. Stained sections were mounted in mounting medium (Vector Laboratories, Burlingame, CA, USA) before imaging. Sometimes, nuclei were counterstained with 1 μM TO-PRO-3 dye (Invitrogen).

For histology sections, embryos were fixed in Bouin's solution (Sigma-Aldrich, St Louis, MO, USA) and embedded in JB-4 plastic resin polymer (Polysciences, Warrington, PA, USA). Blocks were sectioned (7 μm) using a Leica RM2265 microtome. Sections were dried on a heating plate and stained with Hematoxylin and Eosin (Sigma-Aldrich).

Alcian Blue staining

Larvae at 5 dpf were fixed in 4% paraformaldehyde in PBS at 4°C overnight, washed in PBS, and bleached in 10% H_2O_2/0.5% KOH for 1 hour at room temperature (RT). Bleached embryos were washed twice in PBS and incubated in Alcian Blue solution (0.1% Alcian Blue, 70% ethanol, 1% HCl) overnight at RT. Embryos were then washed once in acidic ethanol (70% ethanol, 5% HCl) and cleared in acidic ethanol overnight. Embryos were dehydrated through increasing ethanol concentrations (85 to 100%), transferred to 80% glycerol and stored at 4°C.

Cell death detection

TUNEL assays were performed using the In Situ Cell Death Detection Kit (Roche Diagnostics) following the manufacturer's instructions with the modification that the TUNEL reaction (1 hour at 37°C) was stopped by incubation in 300 mM sodium chloride/30 mM sodium citrate for 15 minutes at RT. Acridine Orange staining was performed by incubating live embryos in 2 μg/ml Acridine Orange (Sigma-Aldrich) in E3 medium (5 mM NaCl, 0.17 mM KCl, 0.4 mM $CaCl_2$, 0.16 mM $MgSO_4$) for 30 minutes at RT. Embryos were washed with E3 medium twice for 10 minutes each before imaging.

Microinjections

One-cell stage embryos from *gle1*$^{hi4161a/+}$ intercrosses were injected with a mix of two non-overlapping morpholino antisense oligonucleotides (MOs) designed to block the translation of *gle1*: *drgle1ATG1*, 5′-TCAGAAGGCATTTTGAGGGCATTAA-3′; and *drgle1UTR1*, 5′-ACACCTTTAGCAGCCCAAACAAGCC-3′; 1.5 ng each MO per embryo (Gene Tools). Five-nucleotide-mismatched MOs were used as controls. Pipettes were pulled on a micropipette puller (Model P-2000, Sutter Instruments, Novato, CA, USA). Injections were performed with an air-injection apparatus (Pneumatic PicoPump PV820, World Precision Instruments, Sarasota, FL, USA). The injected volume (typically ~1 nl) was measured with a microruler.

In rescue assays, capped human *GLE1b* mRNAs were prepared using the mMessage mMachine RNA Synthesis Kit (Ambion, Carlsbad, CA, USA) following the manufacturer's instructions and injected into one-cell stage embryos, which were first injected with *gle1* MOs. For each MO knockdown and rescue experiment, embryos from the same clutch were used as experimental subjects and controls. Approximately 140 pg of capped RNA was injected per embryo unless stated otherwise.

Transgenesis

To label motoneurons, we used *Tol2*-mediated transgenesis (Kawakami, 2004; Kwan et al., 2007) to generate lines in which TagRFP-T or a histone variant H2AFV-fused TagRFP-T (H2A-TagRFP-T) was expressed from zebrafish *mnx1* upstream elements. Mixtures of 25 pg of the transgenesis plasmid and 25 pg transposase mRNA were injected into wild-type one-cell stage embryos. Injected founders were raised and progeny were screened for the respective transgenesis markers to establish *Tg(mnx1:TagRFP-T)* and *Tg(mnx1:H2A-TagRFP-T)* lines.

Cell transplantations

Wild-type and *gle1* MO-injected embryos from *gle1*$^{hi4161a/+}$ intercrosses were used. Donor and host embryos contain *mnx1:GFP* and *mnx1:TagRFP-T* transgenes, respectively, to differentially label motoneurons in the resulting chimeras. At blastula stage, ~40 cells were transplanted from donor embryos to host embryos with a pulled needle connected to an oil-filled syringe (CellTram Vario Microinjector, Eppendorf, Hauppauge, NY, USA). After transplantation, donor-host pairs were raised individually in 48-well plates. Hosts with GFP$^+$ and TagRFP-T$^+$ motoneurons were imaged at 3 dpf.

Imaging and data processing

Embryos subjected to whole-mount in situ hybridization or Alcian Blue staining were mounted in a bridged slide containing one drop of 80% glycerol, coverslipped and imaged using a Zeiss Axio Imager Z1 microscope equipped with a Zeiss AxioCam MRm digital camera. JB-4 plastic sections were mounted in Cytoseal XYL mounting medium (Richard-Allan Scientific, Kalamazoo, MI, USA) and imaged as above. For live imaging, embryos were anesthetized with 0.03% Tricaine (Sigma-Aldrich) and mounted in 0.8% low-melting-point agarose (SeaPlaque GTG agarose, Lonza, Basel, Switzerland) on glass-bottomed 35-mm dishes (MatTek, Ashland, MA, USA). Live embryos and immunostained cryosections were imaged using 20× (0.7 NA) and 63× (1.4 NA) oil-immersion objectives, respectively, using a Leica TCS SP5 laser-scanning confocal microscope. Confocal images were processed using LAS AF (Leica) and ImageJ (NIH, USA) software. Single optical sections were exported as TIFF files. Brightness and contrast were adjusted (if necessary) using Adobe Photoshop CS5 in accordance with journal policy. Figures were composed with Adobe Illustrator CS5. Statistical analyses (e.g. unpaired *t*-test) were performed and graphed using Prism4 (GraphPad, La Jolla, CA, USA) software. Statistical significance was set at $P<0.005$.

RESULTS

gle1 is widely expressed during zebrafish early development

Through Ensembl database searches, we identified *gle1* in the zebrafish (*Danio rerio*) genome as the sole ortholog of human *GLE1*. By reverse transcriptase PCR (RT-PCR), we isolated coding sequences corresponding to both zebrafish Gle1 isoforms from the total RNA of wild-type embryos (supplementary material Fig. S1). Zebrafish *gle1* and human *GLE1* (Kendirgi et al., 2003) have an identical exon-intron organization and both are predicted to encode two protein isoforms from alternatively spliced transcripts. In addition, the predicted translated gene products of zebrafish *gle1* share high degrees of similarity with the corresponding human GLE1 proteins (50% identity and 69% similarity). RT-PCR and in situ hybridization experiments showed that *gle1* transcripts are maternally inherited and widely expressed from the one-cell stage through 5 days post-fertilization (dpf) (Fig. 1; data not shown). From 48 hours post-fertilization (hpf), *gle1* was prominent in the CNS, eyes, pharyngeal arches, fin buds and digestive system (Fig. 1J,K).

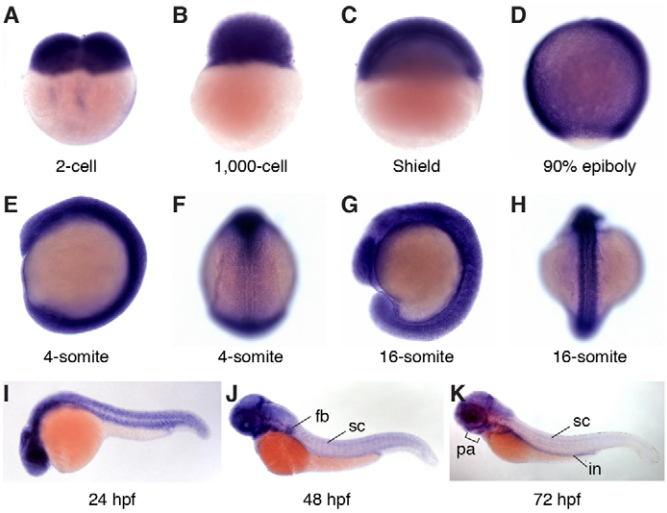

Fig. 1. Expression patterns of zebrafish *gle1* transcripts. (**A-K**) Whole-mount RNA in situ hybridization shows that zebrafish *gle1* transcripts are maternally deposited and ubiquitously expressed during early development (through 24 hpf). From 48 hpf, *gle1* is prominent in the CNS, eyes, pharyngeal arches (pa), fin buds (fb) and intestine (in). F and H show dorsal views; all other panels show lateral views. sc, spinal cord.

Zebrafish *gle1*$^{hi4161a/hi4161a}$ mutants have LCCS1-like phenotypes

To analyze the consequences of Gle1 loss of function, we used an insertional mutant line, *gle1*^{hi4161a} (Amsterdam et al., 2004), in which a provirus was integrated 34 bp downstream of the *gle1* translation start codon, resulting in a non-functional *gle1* allele (supplementary material Fig. S1). Homozygous *gle1*$^{hi4161a/hi4161a}$ embryos (designated *gle1*$^{-/-}$) were initially indistinguishable from their wild-type or heterozygous siblings. However, a spectrum of morphological anomalies was observed at ~48 hpf, including smaller head and eyes (Fig. 2B,D, arrowheads), underdeveloped pectoral fins (Fig. 2D, arrow) and cell death in the head and spinal cord (Fig. 2F, arrow and inset). Some also displayed upward or downward body axis curvatures, which were maintained or exacerbated with time (Fig. 2J). By 5 dpf, *gle1*$^{-/-}$ larvae developed pronounced pleiotropic phenotypes, including small eyes (Fig. 2J; supplementary material Fig. S2A), pericardial and subcutaneous edema (Fig. 2J,L, asterisks), unfolded intestinal epithelia (Fig. 2L, arrowhead) and a distinct craniofacial defect. For the latter, the ventral viscerocranium, which consists of a series of seven pharyngeal arch cartilages (Schilling, 1997), was almost absent, whereas the dorsal neurocranium was still largely intact (compare Fig. 2H with 2G). This phenotype corresponds to the small jaw defect (micrognathia) of human LCCS1 patients.

In addition, *gle1*$^{-/-}$ mutants also became increasingly immotile with time, displayed little spontaneous swimming and were insensitive to touch (data not shown). By measuring the size of spinal transverse sections, we further found that the spinal cord of 5-dpf *gle1*$^{-/-}$ larvae was ~73% of that of the wild type (Fig. 2K,L; supplementary material Fig. S2B). This spinal atrophy phenotype highly resembled the degeneration of spinal cord reported in LCCS1 (Herva et al., 1988).

Taken together, the variety of morphological phenotypes observed in zebrafish *gle1*$^{-/-}$ embryos and early larvae, which include immobility, micrognathia-like craniofacial defects and diminished spinal cords, paralleled characteristic pathologies observed in LCCS1 human fetuses. Thus, we concluded that the zebrafish *gle1*$^{-/-}$ mutant is an excellent model system for studying LCCS1.

Loss of Gle1 activity results in motoneuron defects

Because loss of anterior-horn motoneurons and their descending tracts in the spinal cord is a hallmark of LCCS1 pathology (Herva et al., 1988), we examined motoneuron development in *gle1*$^{-/-}$ embryos. To directly visualize zebrafish motoneurons, we crossed the *gle1*$^{hi4161a/+}$ line with *Tg(mnx1:GFP)* (formerly *hb9:GFP*) (Flanagan-Steet et al., 2005) or *Tg(mnx1:TagRFP-T)* (this study) fish, in which spinal motoneurons and their processes were robustly labeled with GFP or the red fluorescent protein TagRFP-T (Shaner et al., 2008), respectively. In these transgenic lines, motoneuron development was compared between wild-type and *gle1*$^{-/-}$ backgrounds. At 1 dpf, motoneuron development in *gle1*$^{-/-}$ embryos was indistinguishable from that in wild-type embryos. However, at 2 dpf, and similar to the timing of the onset of morphological defects, *gle1*$^{-/-}$ embryos started to show motoneuron defects. Notably, *gle1*$^{-/-}$ embryos had fewer spinal motoneurons

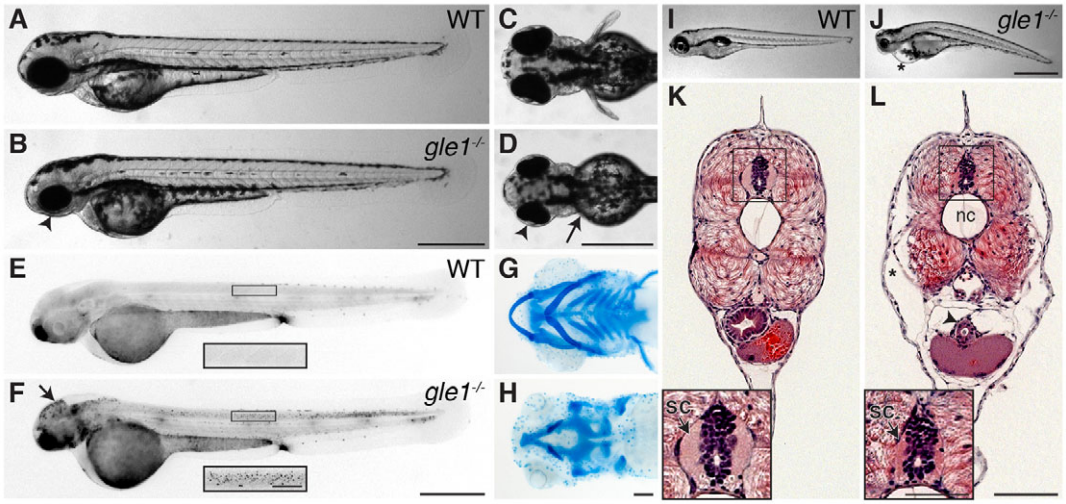

Fig. 2. Morphological phenotypes of *gle1*$^{-/-}$ mutants. (**A-D**) Lateral (A,B) and dorsal (C,D) views of wild-type (A,C) and *gle1*$^{-/-}$ (B,D) zebrafish embryos at 2 dpf. Arrowheads (B,D) mark the smaller head and eyes; arrow (D) marks underdeveloped pectoral fins. (**E**,**F**) Acridine Orange-stained 2 dpf wild-type (E) and *gle1*$^{-/-}$ (F) embryos. Cell death is noted in the head (F, arrow) and spinal cord (F, inset). (**G**,**H**) Alcian Blue-stained head cartilages of 5-dpf wild-type (G) and *gle1*$^{-/-}$ (H) larvae. *gle1*$^{-/-}$ mutant lacks most viscerocranium but has relatively intact neurocranium. (**I**,**J**) Lateral views of 5-dpf wild-type (I) and *gle1*$^{-/-}$ (J) larvae. Asterisk (J) marks pericardial edema. (**K**,**L**) Hematoxylin and Eosin (H&E)-stained transverse sections of wild-type (K) and *gle1*$^{-/-}$ (L) larvae at 5 dpf. *gle1*$^{-/-}$ mutant has a smaller spinal cord (L, arrow in inset). Asterisk (L) marks subcutaneous edema; arrowhead (L) marks unfolded intestine. nc, notochord; sc, spinal cord. Scale bars: 500 μm in B,D,F,J; 100 μm in H,L and F inset; 50 μm in L inset.

than their wild-type siblings, as revealed by fewer GFP-labeled or TagRFP-T-labeled cells in the spinal cord (Fig. 3B, bracket). We also quantified the population size of motoneurons and compared it with that of Rohon-Beard sensory neurons by anti-Islet1/2 staining (Korzh et al., 1993). In agreement with the observation from *mnx1*:GFP/TagRFP-T-labeled *gle1*$^{-/-}$ embryos, anti-Islet1/2 staining revealed that *gle1*$^{-/-}$ embryos had ~25% fewer motoneurons than their wild-type siblings (P<0.0001, unpaired t-test) at 2 dpf. However, there was no significant difference in Rohon-Beard sensory neuron number between *gle1*$^{-/-}$ and wild-type embryos (P>0.09, unpaired t-test) (Table 1; supplementary material Fig. S3). These results indicate that at 2 dpf the population size of spinal motoneurons is selectively affected by reduced Gle1 activity.

In addition to fewer motoneurons, *gle1*$^{-/-}$ embryos also exhibited defects in motor axon arborization at 2 dpf. Compared with wild type, within the trunk muscle the motor axon arbors in *gle1*$^{-/-}$ embryos consistently lacked rostrally projecting nerves around the horizontal myoseptum (Fig. 3B,D). This phenotype was not due to developmental delay because the lack of rostral nerves never recovered as the embryos developed further. Moreover, the horizontal myoseptum appeared intact, suggesting that there was no indirect perturbation (supplementary material Fig. S4). Ventrally projecting nerves in *gle1*$^{-/-}$ embryos also appeared disorganized, often showing excessive and ectopic branching (Fig. 3B,D). The motor nerve bundles were also thinner overall in *gle1*$^{-/-}$ embryos.

Collectively, starting at 2 dpf, at least two motoneuron defects were observed in *gle1*$^{-/-}$ embryos: fewer spinal motoneurons and disorganized motor axon arborization.

Knocking down maternal Gle1 activity exacerbates *gle1* mutant phenotypes

Based on the maternally deposited *gle1* transcripts (Fig. 1A), we speculated that the relatively late onset of phenotypes in *gle1*$^{-/-}$ embryos (at 2 dpf, Figs 2, 3) could be due to a maternal Gle1 contribution. To test this, we injected one-cell stage embryos with a mixture of two non-overlapping morpholino antisense oligonucleotides (MOs) designed to block *gle1* translation. We determined the maximal MO concentration that had a negligible phenotypic effect on wild-type embryos. This suboptimal dose was then used with a mixed population of embryos derived from *gle1*$^{+/-}$ intercrosses. Following phenotypic analysis, we genotyped individual embryos and found that *gle1* knockdown in all three possible genotypic backgrounds (+/+, +/– and –/–) had similar effects on morphology and motoneuron number. The *gle1* MO-injected embryos (*gle1* morphants) showed widespread cell death in the CNS as early as 1 dpf (supplementary material Fig. S5D), a full day earlier than *gle1*$^{-/-}$ embryos (Fig. 2F). At 1 dpf, *gle1* morphants also developed fewer motoneurons, but their motor axon trajectories were similar to those of controls (supplementary material compare Fig. S5E with S5F). However, after 2 dpf, *gle1* morphants displayed pronounced defects in motor axon arborization, including the lack of rostrally (Fig. 4B,E) and dorsally (Fig. 4E) projecting nerves and disorganized motor axon trajectories (Fig. 4B,E). Overall, the motoneuron phenotypes in *gle1* morphants were very similar to, but more severe than, those observed in zygotic *gle1*$^{-/-}$ mutants (Fig. 3B,D).

Importantly, several control experiments validated that the exacerbated CNS cell death and motoneuron defects observed in *gle1* morphants were specific to the knockdown of Gle1 activity (maternal and zygotic) and not due to nonspecific off-target effects. First, injecting five-nucleotide-mismatched *gle1* MOs at the same dose as the *gle1* MOs did not cause any perturbations (data not shown; supplementary material Fig. S5A,B,E). Second, the *gle1* morphant phenotypes could be rescued by expressing human GLE1 (see below). Overall, our Gle1 loss-of-function studies indicate that Gle1 activity is required for motoneuron survival and/or formation, as well as for motor axon arborization. Reducing maternal Gle1 activity allows the otherwise milder and later onset phenotypes of zygotic *gle1*$^{-/-}$ mutants to be revealed.

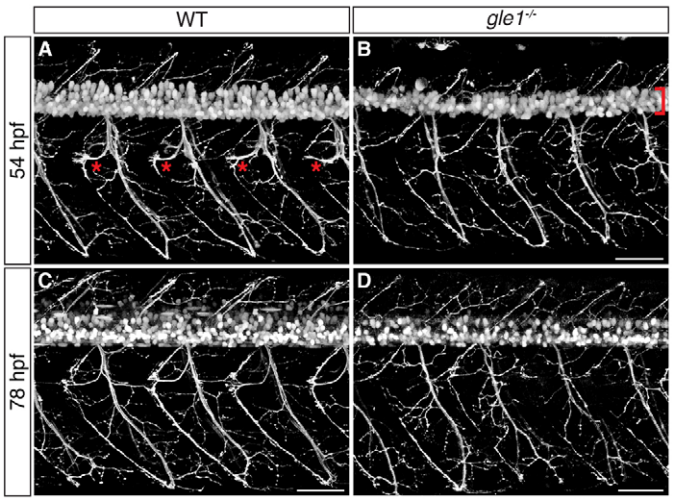

Fig. 3. Motoneuron phenotypes of *gle1*$^{-/-}$ mutants. (**A-D**) Confocal images of live wild-type (A,C) and *gle1*$^{-/-}$ (B,D) zebrafish embryos with motoneurons labeled by *mnx1:GFP* transgene at 54 hpf (A,B) and 78 hpf (C,D). Compared with wild-type siblings, *gle1*$^{-/-}$ embryos have fewer motoneurons in the spinal cord (B, bracket), lack rostrally projecting axons (asterisks in wild type, A) around the horizontal myoseptum, and exhibit disorganized axon arbors and ectopic branching (B,D). The phenotypes are exacerbated with age. Images are lateral views of the trunk spinal cord with dorsal to top, anterior to left. Scale bars: 50 μm.

Secondary motoneurons are severely reduced upon loss of Gle1 function

Zebrafish have two populations of spinal motoneurons: primary motoneurons (PMNs) and secondary motoneurons (SMNs). By 24 hpf, on each side of each segmentally arranged myotomal muscle of the zebrafish trunk, there are three PMNs that are individually classified as CaP, MiP and RoP by the stereotyped positions of their cell bodies and distinct innervation patterns of their axons (Eisen et al., 1986; Myers et al., 1986; Westerfield et al., 1986). Zebrafish SMNs arise later during segmentation and are more numerous than PMNs (Myers et al., 1986; Westerfield et al., 1986). Starting at ~25 hpf, SMNs extend their axons along the paths pioneered by primary axons (Myers, 1985; Pike et al., 1992). Axons of both PMNs and SMNs eventually form the dorsal and ventral motor nerves (Beattie, 2000; Pike et al., 1992).

Based on the phenotypes of 1-dpf *gle1* morphants (supplementary material Fig. S5), we speculated that PMN formation and axogenesis would initiate normally in *gle1* morphants, whereas SMN formation would be compromised. To test whether SMN formation was indeed affected upon the loss of Gle1 activity, we used a zn-8 (Alcama) antibody, which transiently recognizes the somata and fasciculated axons of SMNs but not of PMNs (Fashena and Westerfield, 1999). At 2 dpf in the control embryos, the somata and the fasciculated segments of the rostrally projecting nerves of SMNs were robustly co-labeled by zn-8 antibody and GFP expressed from the *mnx1:GFP* transgene (which labels both PMNs and SMNs) (Fig. 5A-C). By contrast, in *gle1* morphants, the detection of zn-8-positive SMNs was severely reduced (Fig. 5E), whereas the GFP-labeled PMNs were still present (Fig. 5D). These results indicate that attenuation of Gle1 activity severely affects the formation of SMNs but not of PMNs. As such, the SMN perturbation would account for the overall reduction of motoneurons, the thinner axon bundles and the lack of rostrally projecting nerves in the *gle1* mutants and morphants (Figs 3, 4).

Table 1. Number of Rohon-Beard cells and motoneurons in the spinal cord (somites 11-14) at 48 hpf

Genotype	Number of Rohon-Beard cells	Number of motoneurons
Wild type	29.1±1.8 (*n*=8)	235.8±9.2 (*n*=8)
gle1$^{hi4161a/hi4161a}$	25.4±1.1 (*n*=8)	175.1±6.0*** (*n*=8)

Values given ±s.e.m.
***, $P<0.0001$.
n, number of embryos.

Neural precursors, but not newly born neurons, undergo apoptosis upon Gle1 depletion

Given that CNS cell death was one of the earliest phenotypes observed in *gle1* mutants and morphants (Fig. 2F; supplementary material Fig. S5D), we next investigated whether Gle1 depletion causes motoneuron death, thus leading to the observed overall reduction of SMNs. To detect motoneuron death we performed TUNEL (terminal deoxynucleotidyl transferase-mediated dUTP nick end labeling) in *gle1* mutants and morphants, where the motoneuron nuclei were fluorescently labeled by the fusion protein H2A-TagRFP-T expressed from the *mnx1:H2A-TagRFP-T* transgene (see Materials and methods). Surprisingly, the TUNEL assay rarely detected motoneuron death: only 1 out of 108 spinal transverse sections from *gle1* mutants and morphants (*n*=12) showed TUNEL$^+$ H2A-TagRFP-T$^+$ doubly labeled motoneurons (supplementary material Fig. S6, arrows), although TUNEL$^+$ signals were evident in those sections. These results indicate that cells other than motoneurons in the spinal cord die upon Gle1 depletion.

To identify the dying cells in the Gle1-depleted spinal cords, we examined the positions of apoptotic cells relative to other cell types with specific markers. We labeled all postmitotic neurons with anti-Elavl antibody (previously called anti-HuC/D) (Marusich et al., 1994) and apoptotic cells with anti-cleaved caspase 3 antibody. Consistent with the results from the TUNEL assay, anti-cleaved caspase 3 staining revealed pronounced apoptotic cell death in the spinal cord of *gle1* morphants. These apoptotic cells were distributed widely along both the dorsoventral and apical-basal axes of the spinal cord (supplementary material Fig. S7J). Notably, cleaved caspase 3$^+$ cells were often located close to the central canal or immediately adjacent to the basally located Elavl$^+$ cells (examples shown in supplementary material Fig. S7A-I). Strikingly, after extensive examination of samples at different developmental stages (more than 200 spinal transverse sections, *n*=26, at 24, 36 and 52 hpf), we did not find cleaved caspase 3$^+$ Elavl$^+$ doubly labeled cells, indicating that the differentiated neurons did not undergo apoptosis upon Gle1 depletion.

During neurogenesis, neural precursor cells are patterned along the dorsoventral axis of the neural tube, proliferate and then migrate laterally to differentiate into defined neuronal classes (Bylund et al., 2003; Kintner, 2002). The exclusive non-overlapping distribution of cleaved caspase 3$^+$ cells and basally located Elavl$^+$ neurons in *gle1* morphants suggested that at least some of the apoptotic cells might have been neural precursors. Many neural precursors adopt features of radial glia, which give rise to specific classes of neurons in the brain (Anthony et al., 2004; Malatesta et al., 2003; Miyata et al., 2001; Noctor et al.,

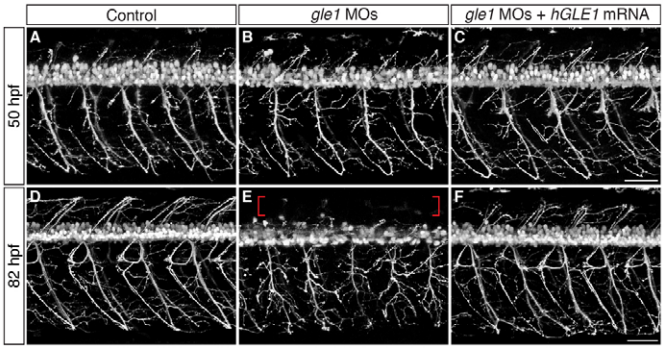

Fig. 4. Motoneuron phenotypes of *gle1* morphants. (**A-F**) Confocal images of live control (A,D) and *gle1* morphant (B,C,E,F) zebrafish embryos with motoneurons labeled by *mnx1:TagRFP-T* transgene at 50 hpf (A-C) and 82 hpf (D-F). *gle1* morphants were injected with buffer alone (B,E) or with ~140 pg in vitro transcribed *EGFP*-tagged human *GLE1b* mRNA (C,F). *gle1* morphants lack rostrally projecting nerves and show pronounced defects in motor axon arborization (B,E), especially at 82 hpf, when the *gle1* morphant also lacks dorsally projecting axons (E, brackets) and aberrations in ventrally projecting axons are particularly evident. Expressing human GLE1 efficiently rescues the arborization defects (C,F). Images are lateral views of the trunk spinal cord with dorsal to top, anterior to left. Scale bars: 50 μm.

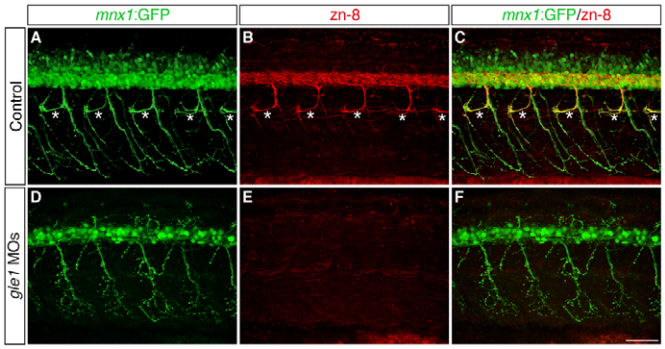

Fig. 5. Secondary motoneurons are severely reduced in *gle1* morphants. (**A-F**) Confocal images of control (A-C) and *gle1* morphant (D-F) zebrafish embryos with motoneurons labeled by *mnx1:GFP* transgene and zn-8 (Alcama) antibody to reveal somata and fasciculated axons of secondary motoneurons at 56 hpf. *gle1* morphants lose most zn-8 immunoreactivity, including the rostrally projecting nerves (asterisks in the control, A-C), but still retain the primary motoneurons (*mnx1*:GFP$^+$) (D,F). Images are lateral views of the trunk spinal cord with dorsal to top, anterior to left. Scale bar: 50 μm.

2002). In the zebrafish spinal cord, a subset of proliferative glial fibrillary acidic protein (Gfap)-positive radial glia reside along the central canal and serve as the neural and glial precursors that develop into motoneurons and oligodendrocytes (Kim et al., 2008). Using the *Tg(gfap:GFP)* line to mark radial glia (Bernardos and Raymond, 2006), we found that more than 70% of cleaved caspase 3$^+$ cells in the spinal cord of *gle1* morphants (n=23) were also Gfap$^+$; many of those cells were located along the central canal (examples shown in Fig. 6A-L, arrows). We also observed some Elavl$^+$ Gfap$^+$ cells as previously described (Kim et al., 2008). GFP is stable and its fluorescence can persist after the transgene is no longer transcribed. Thus, the newly differentiated neurons (Elavl$^+$) derived from Gfap$^+$ radial glia might be GFP$^+$. Furthermore, we found that almost all Gfap$^+$ radial cells in the spinal cord expressed Sox2, a known neural stem cell marker (Bylund et al., 2003; Graham et al., 2003) (supplementary material Fig. S8A-D). Sox2$^+$ cells were close to the apical surface and were mutually exclusive with motoneurons and Elavl$^+$ neurons (supplementary material Fig. S8E-P; data not shown). Thus, the distribution of Sox2$^+$ neural precursors highly resembles that of the apoptotic cells in Gle1-depleted spinal cords, suggesting that these two populations extensively overlap. Indeed, TUNEL and anti-Sox2 double labeling revealed TUNEL$^+$ Sox2$^+$ doubly labeled cells in the spinal cord upon Gle1 depletion (Fig. 6Q-T, arrowheads), confirming that Sox2$^+$ neural precursors die upon Gle1 depletion. Taken together, we conclude that neural precursor cells, rather than differentiated neurons, undergo apoptosis upon Gle1 depletion.

To address whether defects in cell division underlie the death of Gle1-depleted neural precursors, we examined cell cycle progression of spinal neural precursors in the control and *gle1* morphant embryos using a 'percent labeled mitoses' paradigm (Locker et al., 2006) (supplementary material Fig. S9). The control and Gle1-depleted neural precursors progressed through the cell cycle at a similar rate between 26 and 33 hpf (~3.5 hours per cycle). After 33 hpf, the majority of neural precursors in the control embryos exited the cell cycle and transitioned into differentiation. However, ~80% of Gle1-depleted precursors proceeded through a full cell cycle between 32 and 36 hpf (compared with fewer than 10% of controls) (supplementary material Fig. S9D). Thus, Gle1-depleted neural precursors failed to exit the cell cycle and/or transition into differentiation. Such a failure might trigger apoptosis of Gle1-deficient neural precursors.

Gle1 acts non-cell-autonomously in motor axon arborization

In addition to impaired neurogenesis, Gle1 depletion also led to aberrant motor axon outgrowth. Given that an active crosstalk between neurons and their environment is required for navigating axons to form correct arborization patterns (for reviews, see Beattie, 2000; Chisholm and Tessier-Lavigne, 1999), Gle1 could be required intrinsically in motoneurons and/or extrinsically in the environment for proper axon arborization. To distinguish between these possibilities, we performed mosaic analyses of chimeras generated by cell transplantation. To increase the robustness of obtaining desired chimeras, we used *gle1* morphants as donors or hosts. We further employed donor and host embryos with motoneurons labeled by *mnx1:GFP* and *mnx1:TagRFP-T* transgenes, respectively, to enable observation of donor and host motor axon behaviors in the same chimeras simultaneously.

Transplantation of wild-type donor cells (*mnx1*:GFP$^+$) into *gle1* morphant hosts (*mnx1*:TagRFP-T$^+$) revealed that GFP$^+$ wild-type motoneurons primarily followed the aberrant motor axon trajectories of TagRFP-T$^+$ motoneurons in the *gle1* morphant hosts (Fig. 7B; n=10 chimeras). These results indicate that Gle1 activity is required in the environment for normal motor axon arborization; wild-type intrinsic Gle1 activity in the motoneurons is not sufficient. Conversely, when the donor cells from *gle1* morphants were transplanted into wild-type hosts, the resulting *gle1* morphant-derived motoneurons consistently exhibited the normal axon arborization patterns (GFP$^+$) of their neighboring wild-type motor axons (TagRFP-T$^+$) (Fig. 7C; n=17 chimeras). Notably, the rostrally projecting axons now developed from the cells of *gle1*

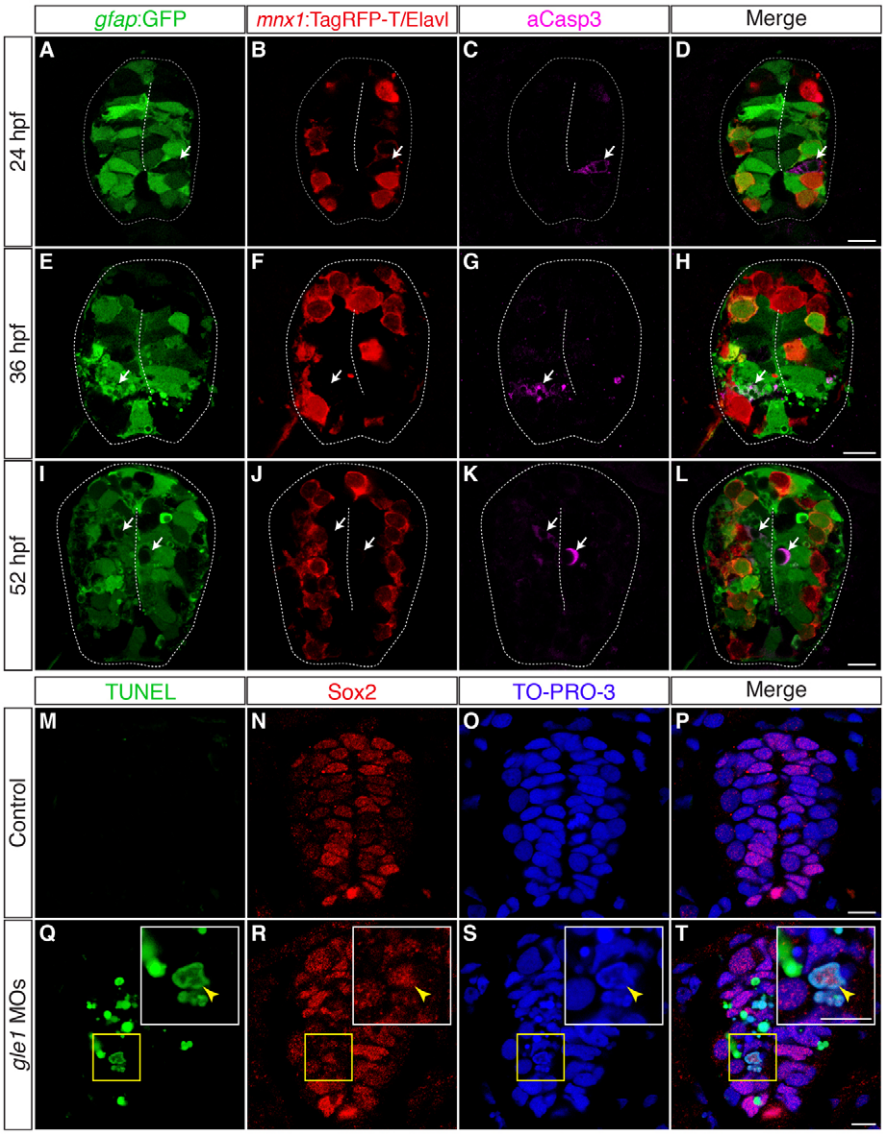

Fig. 6. Neural precursors, rather than differentiated neurons, undergo apoptosis in *gle1* morphants. (**A-L**) Transverse cryosections through the spinal cords of *gle1* morphants harboring *gfap:GFP* and *mnx1:TagRFP-T* transgenes were stained with anti-Elavl and anti-cleaved caspase 3 (aCasp3) antibodies at 24 (A-D), 36 (E-H) and 52 (I-L) hpf. The *gfap:GFP* transgene reveals the radial glia (A,E,I); anti-Elavl staining reveals newly differentiated neurons with a cytoplasmic signal; the *mnx1:TagRFP-T* transgene labels motoneurons with both nuclear and cytoplasmic signals (B,F,J); aCasp3 labels apoptotic cells (C,G,K). aCasp3$^+$ cells are often *gfap*:GFP$^+$ (arrows), located close to the central canal (dashed lines), and/or in close proximity with Elavl$^+$ *mnx1*:TagRFP-T$^+$ neurons. Elavl$^+$ *mnx1*:TagRFP-T$^+$ neurons are always negative for aCasp3 (merged channels, D,H,L). (**M-T**) Transverse cryosections through the spinal cords of control (M-P) and *gle1* morphant (Q-T) embryos at 31 hpf were stained for Sox2, followed by TUNEL reactions, to reveal Sox2$^+$ neural precursors (N,R) and TUNEL$^+$ apoptotic cells (M,Q). Nuclei were counterstained with TO-PRO-3 (O,S). Detection of Sox2$^+$ TUNEL$^+$ nuclei (arrowheads) indicates that Sox2$^+$ neural precursors die upon Gle1 depletion. Each image is a single optical section (~1 μm) extracted from the confocal *z*-stack (dorsal to top). Dashed lines outline spinal cords and central canals. Scale bars: 10 μm in D,H,L; 7.5 μm in P,T.

morphant donors (Fig. 7C, asterisks). This was in stark contrast to the phenotypes observed in *gle1* mutants or morphants, in which the rostrally projecting axons failed to form (Figs 3, 4). These results further indicated that Gle1 acts in a non-cell-autonomous manner during motor axon arborization.

Wild-type human GLE1, but not the Fin_{Major} mutant form, rescues the zebrafish Gle1 deficiency defects

To directly test the use of zebrafish as a model for studying LCCS1, we investigated the effects of expressing human GLE1 in the *gle1* morphants. The CNS cell death and aberrant axonal trajectories were rescued by co-injecting *gle1* MOs with in vitro transcribed human *GLE1* mRNA (encoding GLE1 that is either untagged or EGFP tagged at the N-terminus) (Fig. 4C,F; supplementary material Fig. S10B,D). To compare the wild-type and Fin_{Major} mutant forms of human GLE1, we assessed the overall consequence of *gle1* MO-induced head cell death – categorized as severe, mild or wild-type-like – after injecting the corresponding human *GLE1* mRNAs. When *gle1* morphants were injected with buffer alone, as expected no rescue of head cell death was observed, with ~75% of *gle1* morphants showing severe head cell death (Fig. 8). Injecting wild-type human *GLE1* mRNA, however, efficiently rescued head cell death, with ~75% of human *GLE1* mRNA-injected *gle1* morphants showing wild-type-like head morphology. In striking contrast, injecting human *GLE1* Fin_{Major} mRNA exhibited very limited, if any, rescuing effect on head cell death (Fig. 8). Western blotting experiments confirmed that the wild-type and Fin_{Major} GLE1 proteins were comparably expressed in the embryos (supplementary material Fig. S11). This cross-species rescue demonstrates that Gle1 function is evolutionarily conserved between human and zebrafish. In addition, this directly supports the use of zebrafish as a model with which to determine the pathophysiological consequences of human LCCS1.

DISCUSSION

Using zebrafish to investigate the function of the *gle1* gene mutated in LCCS1, we have established the first vertebrate model with which to study this human lethal congenital disease. We find that the zebrafish *gle1* mutant and morphant phenotypes parallel several key LCCS1 syndromes. Moreover, expressing human GLE1

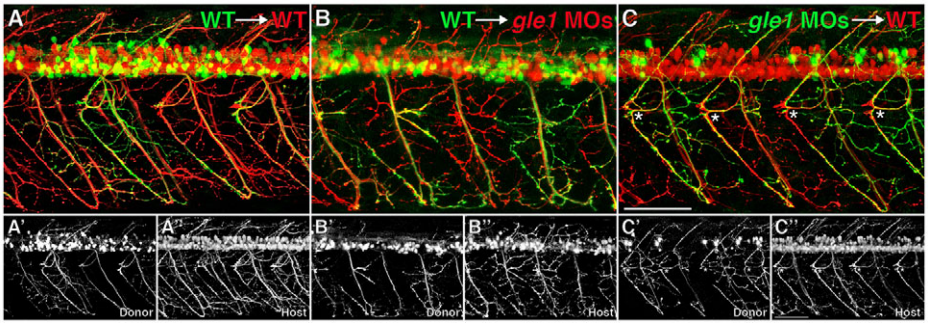

Fig. 7. Gle1 acts non-cell-autonomously in motor axon arborization. (**A-C″**) Confocal images of live chimera embryos at 3 dpf. Cells from either wild-type (A,B) or *gle1* morphant (C) donor embryos (*mnx1*:GFP^{+}) were transplanted into wild-type (A,C) or *gle1* morphant (B) hosts (*mnx1*:TagRFP-T^{+}). Wild-type donor motoneurons extend their axons and follow the aberrant motor axons of the *gle1* morphant host (B). Conversely, motoneurons from the *gle1* morphant donor extend their axons normally in the wild-type host (C) as in the case with the wild type-to-wild type transplantation (A). Rostrally projecting motor nerves from the *gle1* morphant donor are restored in the wild-type environment (asterisks, C). Single-channel images (A′,A″,B′,B″,C′,C″) are shown beneath the merged images to distinctly visualize donor and host axons. Images are lateral views of the trunk spinal cord with dorsal to top, anterior to left. Scale bars: 75 μm.

rescues zebrafish Gle1 deficiency phenotypes, whereas expressing the human GLE1 Fin_{Major} mutant does not. Further analysis of neuronal development shows that lack of Gle1 function directly impacts the survival of neural precursors and motor axon arborization. Surprisingly, differentiated neurons (e.g. those born before maternal Gle1 is depleted) rarely die upon Gle1 depletion. These observations are in sharp contrast to conclusions from prior work that proposed that LCCS1 pathology is linked to perturbations of motoneuron development and maturation (Nousiainen et al., 2008). Our studies raise the possibility that

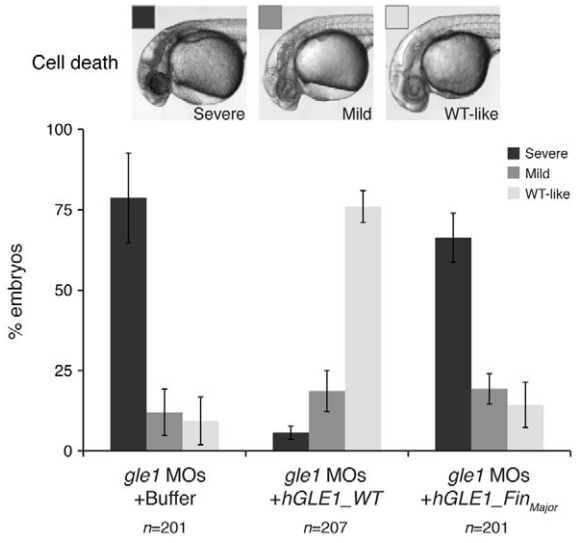

Fig. 8. Wild-type human GLE1, but not the Fin_{Major} mutant form, rescues the defects caused by Gle1 depletion. Embryos from *gle1*$^{hi4161a/+}$ intercrosses were injected with a mix of two non-overlapping *gle1* translation-blocking morpholinos (*gle1* MOs). Following MO injection, the embryos were injected with buffer alone (*gle1* MOs + Buffer) or with ~140 pg of in vitro transcribed human *GLE1* mRNA (wild type, *gle1* MOs + *hGLE1_WT*; or the Fin_{Major} mutant form, *gle1* MOs + *hGLE1_*Fin_{Major}) at the one-cell stage. The extent of head cell death – categorized as severe, mild or wild-type-like (WT-like) – was scored at 32 hpf. Only injecting wild-type *GLE1* mRNA, but not the Fin_{Major} mutant form, rescues the head cell death. At least three independent injections were performed for each condition. Values are mean ± s.e.m. *n*, number of embryos analyzed in each condition.

susceptibility of highly proliferative cells to Gle1 deficiency, including organ precursors, constitutes the cellular basis of pleiotropic phenotypes in LCCS1.

This new interpretation of the LCCS1 pathophysiology also uncovers important links between critical developmental events and specific steps in the molecular regulation of gene expression. Gle1 is essential for mRNA export (Kendirgi et al., 2003; Murphy and Wente, 1996; Watkins et al., 1998) and also regulates translation (Bolger et al., 2008). In highly proliferative cells, Gle1 roles in mRNA export and translation could be crucial to support a high rate of protein synthesis. During mRNA export at nuclear pore complexes (NPCs), Gle1 binds inositol hexakisphosphate (IP_6) and the Gle1-IP_6 complex facilitates ATP loading and activation of Dbp5 (Alcazar-Roman et al., 2006; Noble et al., 2011; Weirich et al., 2006). Dbp5 is an essential RNA-dependent ATPase of the DEAD-box protein family (Schmitt et al., 1999; Snay-Hodge et al., 1998; Tseng et al., 1998). Members of this DEAD-box protein family serve as RNA helicases and/or RNA-protein complex remodelers during many essential aspects of RNA metabolism (Cordin et al., 2006; Jankowsky, 2011; Jankowsky and Bowers, 2006; Linder, 2006; Rocak and Linder, 2004). For Dbp5, conversion to the ADP-bound conformation triggers the release of proteins from the mRNA during export and potentially during translation termination (Gross et al., 2007; Noble et al., 2011; Tran et al., 2007). The Dbp5 cycles of ATP hydrolysis at the NPC are controlled by both Gle1-IP_6 and an NPC-localized ADP release factor, Nup159 (Hodge et al., 2011; Noble et al., 2011). In addition to working with IP_6 and Dbp5 during mRNA export and translation termination, Gle1 also mediates translation initiation in an IP_6- and Dbp5-independent manner (Bolger et al., 2008; Bolger and Wente, 2011). With Gle1 being a key regulator during multiple phases of mRNA metabolism, we speculate that loss of Dbp5 function or IP_6 production might have similar developmental and disease impacts to Gle1 disruption. Analysis of zebrafish null mutants for either *dbp5* (*ddx19* – Zebrafish Information Network) or *ipk1* (*ippk* – Zebrafish Information Network; the kinase responsible for IP_6 generation) has not been reported. We have previously characterized a zebrafish *ipk1* morphant with early developmental defects linked to ciliary function (Sarmah et al., 2005; Sarmah et al., 2007); however, given the high binding affinity of Gle1 for IP_6 (Alcazar-Roman et al., 2010), a zebrafish *ipk1* null is needed to test whether the complete loss of IP_6 production phenocopies the

gle1$^{-/-}$ mutant. Unfortunately, a mouse null for *Ipk1* is embryonic lethal prior to day 8.5 (Verbsky et al., 2005), making it difficult to pinpoint specific developmental defects.

Although Gle1 is an essential regulator of several distinct steps of the mRNA life cycle, it remains unclear whether Gle1 is required at the same levels in different cell types and at different developmental stages. Our zebrafish studies reveal ubiquitous *gle1* expression through early developmental stages, supporting a general requirement of Gle1. However, after 1 dpf, *gle1* expression appears more restricted to certain tissues. Of note, these tissues with prominent *gle1* expression are the same as those that show the most pronounced phenotypes in *gle1* mutants at later stages. Furthermore, these *gle1*-enriched tissues are those that maintain populations of highly proliferative cells at early larval stages (e.g. 3 dpf) (de Jong-Curtain et al., 2009). Therefore, we propose that although Gle1 is likely to be required in all cells, highly proliferative cells demand a higher level of Gle1 to support the robust metabolic activity required during proliferation. Thus, these cells/tissues are the most vulnerable to disruption of Gle1 function and consequently exhibit the most severe phenotypes.

In addition to neuronal deficiency, Gle1-depleted embryos exhibit impaired motor axon arborization in the trunk. There are a plethora of receptor-ligand interactions between neurons and the environment that are required for outgrowing axons to find their correct synaptic targets and to form stereotyped axon arbors (Chisholm and Tessier-Lavigne, 1999). It is therefore surprising that Gle1 activity in the environment appears sufficient to restore normal axon arbors to Gle1-depleted motoneurons. These data further support the idea that Gle1 is required differentially in different tissues. An exciting future challenge will be to identify the cues provided by the wild-type environment and understand how they help organize motor axon arborization. Alternatively, the establishment of normal trajectories of Gle1-depleted motoneurons in the wild-type hosts could be explained by axon fasciculation. The trajectories are laid down by PMNs and are followed by SMN axons. Gle1-depleted motor axons could retain the ability to follow the normal PMN axon trajectories, resulting in normal motor axon arbors.

Multiple insights have been gained from our molecular and pathological analyses of *gle1* in zebrafish. In terms of the molecular mechanism, the major mutation in LCCS1 patients, Fin_{Major}, is a three amino acid insertion in the putative coiled-coil domain of human GLE1 (Nousiainen et al., 2008; Watkins et al., 1998). To date, several Gle1 interaction partners have been identified. Gle1 associates with the NPC through interaction with nucleoporin 42 (Nup42) in yeast (Murphy and Wente, 1996; Strahm et al., 1999) or with hCG1 (the human ortholog of Nup42) and NUP155 in human cells (Kendirgi et al., 2005; Rayala et al., 2004). Gle1 also directly binds IP_6 (Alcazar-Roman et al., 2010; Alcazar-Roman et al., 2006; Montpetit et al., 2011; Weirich et al., 2006). However, the domain corresponding to the Fin_{Major} insertion is not required for interaction with IP_6, Nup42/hCG1 or NUP155 (Alcazar-Roman et al., 2010; Kendirgi et al., 2005; Rayala et al., 2004). Thus, the perturbation could impact a novel interaction partner involved in mRNA export or translation. Alternatively, the Fin_{Major} mutation might instead be a functionally null allele, as we find no significant rescue of the head cell death phenotype when human Fin_{Major} is expressed in zebrafish *gle1* morphants. Additional studies are needed to determine whether the Fin_{Major} mutation disrupts only a subset of Gle1 functions (mRNA export and/or translation). The zebrafish rescue assay developed here provides a valuable in vivo system with which to further test *gle1* disease alleles.

We propose that the wide spectrum of LCCS1 syndromes is of both neurogenic and non-neurogenic origin. Furthermore, the manifestation of phenotypes could be directly correlated with the high demand for Gle1 in highly proliferative cells. For the neurogenic aspect of the disease, apoptosis of neural precursors, not of differentiated neurons, might be the underlying cause of spinal cord atrophy. This in turn would lead to fetal immobility and, ultimately, multiple joint contractures, phenotypes that are often secondary to immobility (Moessinger, 1983). As for phenotypes such as edema, micrognathia and underdeveloped organs, we speculate that they are of non-neurogenic origin. However, as in the case of neuronal tissues, these non-neuronal defects could be caused by death of corresponding organ precursors. In support of the latter, we find that proliferative domains of these tissues in zebrafish, including the ciliary marginal zone of the eyes (supplementary material Fig. S2A), intestinal epithelia (Fig. 2L) and pharyngeal arches (data not shown), all show signs of apoptosis upon the loss of Gle1 activity.

In summary, we have provided the first insight into the functional consequences of *gle1* mutations in vertebrate development and LCCS1 pathology. The fact that the etiology of motoneuron defects in LCCS1 is developmental and not neurodegenerative in origin, sets the stage for considering strategies that might rescue such defects.

Acknowledgements

We gratefully acknowledge Watson Folk for technical assistance; Wenbiao Chen, Josh Gamse, Ela Knapik, Lila Solnica-Krezel and Wen-Der Wang for sharing reagents and advice; the Zebrafish International Resource Center (supported by NIH P40 RR012546); Koichi Kawakami for *Tol2* transposon system; Chi-Bin Chien for Gateway plasmids; Dirk Meyer for *mnx1*:GFP line and constructs; and Wente laboratory members for discussions. Monoclonal antibodies 39.4D5 and zn-8 (developed by T. M. Jessell, S. Brenner-Morton and B. Trevarrow) were obtained from the Developmental Studies Hybridoma Bank (NICHD supported and maintained by The University of Iowa, Department of Biology, Iowa City, IA 52242, USA).

Funding

This work was supported by the March of Dimes Foundation [FY-10-360 to S.R.W.]; and the National Institutes of Health [R37 GM051219 to S.R.W.]. Deposited in PMC for release after 12 months.

Competing interests statement

The authors declare no competing financial interests.

Supplementary material

Supplementary material available online at
http://dev.biologists.org/lookup/suppl/doi:10.1242/dev.074344/-/DC1

References

Alcazar-Roman, A. R., Tran, E. J., Guo, S. and Wente, S. R. (2006). Inositol hexakisphosphate and Gle1 activate the DEAD-box protein Dbp5 for nuclear mRNA export. *Nat. Cell Biol.* **8**, 711-716.

Alcazar-Roman, A. R., Bolger, T. A. and Wente, S. R. (2010). Control of mRNA export and translation termination by inositol hexakisphosphate requires specific interaction with Gle1. *J. Biol. Chem.* **285**, 16683-16692.

Amsterdam, A., Nissen, R. M., Sun, Z., Swindell, E. C., Farrington, S. and Hopkins, N. (2004). Identification of 315 genes essential for early zebrafish development. *Proc. Natl. Acad. Sci. USA* **101**, 12792-12797.

Anthony, T. E., Klein, C., Fishell, G. and Heintz, N. (2004). Radial glia serve as neuronal progenitors in all regions of the central nervous system. *Neuron* **41**, 881-890.

Beattie, C. E. (2000). Control of motor axon guidance in the zebrafish embryo. *Brain Res. Bull.* **53**, 489-500.

Bernardos, R. L. and Raymond, P. A. (2006). GFAP transgenic zebrafish. *Gene Expr. Patterns* **6**, 1007-1013.

Bolger, T. A. and Wente, S. R. (2011). Gle1 is a multifunctional DEAD-box protein regulator that modulates Ded1 in translation initiation. *J. Biol. Chem.* **286**, 39750-39759.

Bolger, T. A., Folkmann, A. W., Tran, E. J. and Wente, S. R. (2008). The mRNA export factor Gle1 and inositol hexakisphosphate regulate distinct stages of translation. *Cell* **134**, 624-633.

Braman, J., Papworth, C. and Greener, A. (1996). Site-directed mutagenesis using double-stranded plasmid DNA templates. *Methods Mol. Biol.* **57**, 31-44.
Bylund, M., Andersson, E., Novitch, B. G. and Muhr, J. (2003). Vertebrate neurogenesis is counteracted by Sox1-3 activity. *Nat. Neurosci.* **6**, 1162-1168.
Chisholm, A. and Tessier-Lavigne, M. (1999). Conservation and divergence of axon guidance mechanisms. *Curr. Opin. Neurobiol.* **9**, 603-615.
Cordin, O., Banroques, J., Tanner, N. K. and Linder, P. (2006). The DEAD-box protein family of RNA helicases. *Gene* **367**, 17-37.
de Jong-Curtain, T. A., Parslow, A. C., Trotter, A. J., Hall, N. E., Verkade, H., Tabone, T., Christie, E. L., Crowhurst, M. O., Layton, J. E., Shepherd, I. T. et al. (2009). Abnormal nuclear pore formation triggers apoptosis in the intestinal epithelium of elys-deficient zebrafish. *Gastroenterology* **136**, 902-911.
Eisen, J. S., Myers, P. Z. and Westerfield, M. (1986). Pathway selection by growth cones of identified motoneurones in live zebra fish embryos. *Nature* **320**, 269-271.
Fashena, D. and Westerfield, M. (1999). Secondary motoneuron axons localize DM-GRASP on their fasciculated segments. *J. Comp. Neurol.* **406**, 415-424.
Flanagan-Steet, H., Fox, M. A., Meyer, D. and Sanes, J. R. (2005). Neuromuscular synapses can form in vivo by incorporation of initially aneural postsynaptic specializations. *Development* **132**, 4471-4481.
Folkmann, A. W., Noble, K. N., Cole, C. N. and Wente, S. R. (2011). Dbp5, Gle1-IP6, and Nup159: a working model for mRNP export. *Nucleus* **2**, 540-548.
Graham, V., Khudyakov, J., Ellis, P. and Pevny, L. (2003). SOX2 functions to maintain neural progenitor identity. *Neuron* **39**, 749-765.
Gross, T., Siepmann, A., Sturm, D., Windgassen, M., Scarcelli, J. J., Seedorf, M., Cole, C. N. and Krebber, H. (2007). The DEAD-box RNA helicase Dbp5 functions in translation termination. *Science* **315**, 646-649.
Hall, J. G. (1985). Genetic aspects of arthrogryposis. *Clin. Orthop. Relat. Res.* **194**, 44-53.
Hall, J. G. (1997). Arthrogryposis multiplex congenita: etiology, genetics, classification, diagnostic approach, and general aspects. *J. Pediatr. Orthop. B* **6**, 159-166.
Herva, R., Leisti, J., Kirkinen, P. and Seppanen, U. (1985). A lethal autosomal recessive syndrome of multiple congenital contractures. *Am. J. Med. Genet.* **20**, 431-439.
Herva, R., Conradi, N. G., Kalimo, H., Leisti, J. and Sourander, P. (1988). A syndrome of multiple congenital contractures: neuropathological analysis on five fetal cases. *Am. J. Med. Genet.* **29**, 67-76.
Hodge, C. A., Tran, E. J., Noble, K. N., Alcazar-Roman, A. R., Ben-Yishay, R., Scarcelli, J. J., Folkmann, A. W., Shav-Tal, Y., Wente, S. R. and Cole, C. N. (2011). The Dbp5 cycle at the nuclear pore complex during mRNA export I: dbp5 mutants with defects in RNA binding and ATP hydrolysis define key steps for Nup159 and Gle1. *Genes Dev.* **25**, 1052-1064.
Jankowsky, E. (2011). RNA helicases at work: binding and rearranging. *Trends Biochem. Sci.* **36**, 19-29.
Jankowsky, E. and Bowers, H. (2006). Remodeling of ribonucleoprotein complexes with DExH/D RNA helicases. *Nucleic Acids Res.* **34**, 4181-4188.
Kawakami, K. (2004). Transgenesis and gene trap methods in zebrafish by using the Tol2 transposable element. *Methods Cell Biol.* **77**, 201-222.
Kendirgi, F., Barry, D. M., Griffis, E. R., Powers, M. A. and Wente, S. R. (2003). An essential role for hGle1 nucleocytoplasmic shuttling in mRNA export. *J. Cell Biol.* **160**, 1029-1040.
Kendirgi, F., Rexer, D. J., Alcazar-Roman, A. R., Onishko, H. M. and Wente, S. R. (2005). Interaction between the shuttling mRNA export factor Gle1 and the nucleoporin hCG1: a conserved mechanism in the export of Hsp70 mRNA. *Mol. Biol. Cell* **16**, 4304-4315.
Kim, H., Shin, J., Kim, S., Poling, J., Park, H. C. and Appel, B. (2008). Notch-regulated oligodendrocyte specification from radial glia in the spinal cord of zebrafish embryos. *Dev. Dyn.* **237**, 2081-2089.
Kimmel, C. B., Ballard, W. W., Kimmel, S. R., Ullmann, B. and Schilling, T. F. (1995). Stages of embryonic development of the zebrafish. *Dev. Dyn.* **203**, 253-310.
Kintner, C. (2002). Neurogenesis in embryos and in adult neural stem cells. *J. Neurosci.* **22**, 639-643.
Korzh, V., Edlund, T. and Thor, S. (1993). Zebrafish primary neurons initiate expression of the LIM homeodomain protein Isl-1 at the end of gastrulation. *Development* **118**, 417-425.
Kwan, K. M., Fujimoto, E., Grabher, C., Mangum, B. D., Hardy, M. E., Campbell, D. S., Parant, J. M., Yost, H. J., Kanki, J. P. and Chien, C. B. (2007). The Tol2kit: a multisite gateway-based construction kit for Tol2 transposon transgenesis constructs. *Dev. Dyn.* **236**, 3088-3099.
Lebenthal, E., Shochet, S. B., Adam, A., Seelenfreund, M., Fried, A., Najenson, T., Sandbank, U. and Matoth, Y. (1970). Arthrogryposis multiplex congenita: twenty-three cases in an Arab kindred. *Pediatrics* **46**, 891-899.
Linder, P. (2006). Dead-box proteins: a family affair-active and passive players in RNP-remodeling. *Nucleic Acids Res.* **34**, 4168-4180.
Locker, M., Agathocleous, M., Amato, M. A., Parain, K., Harris, W. A. and Perron, M. (2006). Hedgehog signaling and the retina: insights into the mechanisms controlling the proliferative properties of neural precursors. *Genes Dev.* **20**, 3036-3048.
Makela-Bengs, P., Jarvinen, N., Vuopala, K., Suomalainen, A., Ignatius, J., Sipila, M., Herva, R., Palotie, A. and Peltonen, L. (1998). Assignment of the disease locus for lethal congenital contracture syndrome to a restricted region of chromosome 9q34, by genome scan using five affected individuals. *Am. J. Hum. Genet.* **63**, 506-516.
Malatesta, P., Hack, M. A., Hartfuss, E., Kettenmann, H., Klinkert, W., Kirchhoff, F. and Gotz, M. (2003). Neuronal or glial progeny: regional differences in radial glia fate. *Neuron* **37**, 751-764.
Marusich, M. F., Furneaux, H. M., Henion, P. D. and Weston, J. A. (1994). Hu neuronal proteins are expressed in proliferating neurogenic cells. *J. Neurobiol.* **25**, 143-155.
Miyata, T., Kawaguchi, A., Okano, H. and Ogawa, M. (2001). Asymmetric inheritance of radial glial fibers by cortical neurons. *Neuron* **31**, 727-741.
Moessinger, A. C. (1983). Fetal akinesia deformation sequence: an animal model. *Pediatrics* **72**, 857-863.
Montpetit, B., Thomsen, N. D., Helmke, K. J., Seeliger, M. A., Berger, J. M. and Weis, K. (2011). A conserved mechanism of DEAD-box ATPase activation by nucleoporins and InsP6 in mRNA export. *Nature* **472**, 238-242.
Murphy, R. and Wente, S. R. (1996). An RNA-export mediator with an essential nuclear export signal. *Nature* **383**, 357-360.
Myers, P. Z. (1985). Spinal motoneurons of the larval zebrafish. *J. Comp. Neurol.* **236**, 555-561.
Myers, P. Z., Eisen, J. S. and Westerfield, M. (1986). Development and axonal outgrowth of identified motoneurons in the zebrafish. *J. Neurosci.* **6**, 2278-2289.
Noble, K. N., Tran, E. J., Alcazar-Roman, A. R., Hodge, C. A., Cole, C. N. and Wente, S. R. (2011). The Dbp5 cycle at the nuclear pore complex during mRNA export II: nucleotide cycling and mRNP remodeling by Dbp5 are controlled by Nup159 and Gle1. *Genes Dev.* **25**, 1065-1077.
Noctor, S. C., Flint, A. C., Weissman, T. A., Wong, W. S., Clinton, B. K. and Kriegstein, A. R. (2002). Dividing precursor cells of the embryonic cortical ventricular zone have morphological and molecular characteristics of radial glia. *J. Neurosci.* **22**, 3161-3173.
Nousiainen, H. O., Kestila, M., Pakkasjarvi, N., Honkala, H., Kuure, S., Tallila, J., Vuopala, K., Ignatius, J., Herva, R. and Peltonen, L. (2008). Mutations in mRNA export mediator GLE1 result in a fetal motoneuron disease. *Nat. Genet.* **40**, 155-157.
Pakkasjarvi, N., Ritvanen, A., Herva, R., Peltonen, L., Kestila, M. and Ignatius, J. (2006). Lethal congenital contracture syndrome (LCCS) and other lethal arthrogryposes in Finland-an epidemiological study. *Am. J. Med. Genet. A* **140**, 1834-1839.
Pike, S. H., Melancon, E. F. and Eisen, J. S. (1992). Pathfinding by zebrafish motoneurons in the absence of normal pioneer axons. *Development* **114**, 825-831.
Rayala, H. J., Kendirgi, F., Barry, D. M., Majerus, P. W. and Wente, S. R. (2004). The mRNA export factor human Gle1 interacts with the nuclear pore complex protein Nup155. *Mol. Cell. Proteomics* **3**, 145-155.
Rocak, S. and Linder, P. (2004). DEAD-box proteins: the driving forces behind RNA metabolism. *Nat. Rev. Mol. Cell Biol.* **5**, 232-241.
Sarmah, B., Latimer, A. J., Appel, B. and Wente, S. R. (2005). Inositol polyphosphates regulate zebrafish left-right asymmetry. *Dev. Cell* **9**, 133-145.
Sarmah, B., Winfrey, V. P., Olson, G. E., Appel, B. and Wente, S. R. (2007). A role for the inositol kinase Ipk1 in ciliary beating and length maintenance. *Proc. Natl. Acad. Sci. USA* **104**, 19843-19848.
Schilling, T. F. (1997). Genetic analysis of craniofacial development in the vertebrate embryo. *BioEssays* **19**, 459-468.
Schmitt, C., von Kobbe, C., Bachi, A., Pante, N., Rodrigues, J. P., Boscheron, C., Rigaut, G., Wilm, M., Seraphin, B., Carmo-Fonseca, M. et al. (1999). Dbp5, a DEAD-box protein required for mRNA export, is recruited to the cytoplasmic fibrils of nuclear pore complex via a conserved interaction with CAN/Nup159p. *EMBO J.* **18**, 4332-4347.
Shaner, N. C., Lin, M. Z., McKeown, M. R., Steinbach, P. A., Hazelwood, K. L., Davidson, M. W. and Tsien, R. Y. (2008). Improving the photostability of bright monomeric orange and red fluorescent proteins. *Nat. Methods* **5**, 545-551.
Snay-Hodge, C. A., Colot, H. V., Goldstein, A. L. and Cole, C. N. (1998). Dbp5p/Rat8p is a yeast nuclear pore-associated DEAD-box protein essential for RNA export. *EMBO J.* **17**, 2663-2676.
Strahm, Y., Fahrenkrog, B., Zenklusen, D., Rychner, E., Kantor, J., Rosbach, M. and Stutz, F. (1999). The RNA export factor Gle1p is located on the cytoplasmic fibrils of the NPC and physically interacts with the FG-nucleoporin Rip1p, the DEAD-box protein Rat8p/Dbp5p and a new protein Ymr 255p. *EMBO J.* **18**, 5761-5777.
Thisse, C. and Thisse, B. (2008). High-resolution in situ hybridization to whole-mount zebrafish embryos. *Nat. Protoc.* **3**, 59-69.
Tran, E. J., Zhou, Y., Corbett, A. H. and Wente, S. R. (2007). The DEAD-box protein Dbp5 controls mRNA export by triggering specific RNA:protein remodeling events. *Mol. Cell* **28**, 850-859.

Tseng, S. S., Weaver, P. L., Liu, Y., Hitomi, M., Tartakoff, A. M. and Chang, T. H. (1998). Dbp5p, a cytosolic RNA helicase, is required for poly(A)+ RNA export. *EMBO J.* **17**, 2651-2662.

Verbsky, J., Lavine, K. and Majerus, P. W. (2005). Disruption of the mouse inositol 1,3,4,5,6-pentakisphosphate 2-kinase gene, associated lethality, and tissue distribution of 2-kinase expression. *Proc. Natl. Acad. Sci. USA* **102**, 8448-8453.

Wang, D., Jao, L. E., Zheng, N., Dolan, K., Ivey, J., Zonies, S., Wu, X., Wu, K., Yang, H., Meng, Q. et al. (2007). Efficient genome-wide mutagenesis of zebrafish genes by retroviral insertions. *Proc. Natl. Acad. Sci. USA* **104**, 12428-12433.

Watkins, J. L., Murphy, R., Emtage, J. L. and Wente, S. R. (1998). The human homologue of Saccharomyces cerevisiae Gle1p is required for poly(A)+ RNA export. *Proc. Natl. Acad. Sci. USA* **95**, 6779-6784.

Weirich, C. S., Erzberger, J. P., Flick, J. S., Berger, J. M., Thorner, J. and Weis, K. (2006). Activation of the DExD/H-box protein Dbp5 by the nuclear-pore protein Gle1 and its coactivator InsP6 is required for mRNA export. *Nat. Cell Biol.* **8**, 668-676.

Westerfield, M. (2000). *The Zebrafish Book. A Guide for the Laboratory Use of Zebrafish (Danio rerio)*. Eugene, OR: University of Oregon Press.

Westerfield, M., McMurray, J. V. and Eisen, J. S. (1986). Identified motoneurons and their innervation of axial muscles in the zebrafish. *J. Neurosci.* **6**, 2267-2277.

Table S1. Primers

Application	Oligo	Sequence (5′ to 3′)
Genotyping primers for *gle1*^{hi4161a} proviral insertion	Universal LTR	AAGACCCCACCTGTAGGTTTGG
	geno_gle1-F	CCACCGACGAAATGAAACAAAT
	geno_gle1-R	CACCCAGTCTGGGCTGTATTTG
Cloning of zebrafish *gle1* isoforms (RT-PCR)	gle1-F	GGGGACAAGTTTGTACAAAAAAGCAGGCTCCACCATGCCTTCTGAAA ACCTTCGGTGG
	gle1a-R	GGGGACCACTTTGTACAAGAAAGCTGGGTATATTGGCGCCGACGTTT ATTCTATATTG
	gle1b-R	GGGGACCACTTTGTACAAGAAAGCTGGGTAGATGATCTCCACCAATC AGGACCTGA
Cloning of *mnx1* upstream elements	mnx1-F	GGGGACAACTTTGTATAGAAAAGTTGTAGGTTTCACACTCATCACTTG GCATCTG
	mnx1-R	GGGGACTGCTTTTTTGTACAAACTTGACTGGCCCACCTCACAAACAGA TTAAC
Cloning of human *GLE1b* (for in vitro transcription)	hsgle1b-F	GGGGACAAGTTTGTACAAAAAAGCAGGCTCCACCATGCCGTCTGAGG GTCGCTGC
	hsgle1b-R	GGGGACCACTTTGTACAAGAAAGCTGGGTATGGAGTGACATCAGGAG CGCCAGAAGGAGGAAG